

Prediction of fully metallic σ -bonded boron framework induced high superconductivity above 100 K in thermodynamically stable Sr_2B_5 at 40 GPa

Xin Yang,^{1,2} Wenbo Zhao,^{1,2,3} Liang Ma,^{1,2,3} Wencheng Lu,¹ Xin Zhong,¹ Yu Xie,^{1,4,*} Hanyu Liu,^{1,2,3,4,†} and Yanming Ma^{1,2,3,‡}

¹Key Laboratory of Material Simulation Methods & Software of Ministry of Education, College of Physics, Jilin University, Changchun 130012, China

²State Key Laboratory for Superhard Materials, College of Physics, Jilin University, Changchun 130012, China

³International Center of Future Science, Jilin University, Changchun 130012, China

⁴Key Laboratory of Physics and Technology for Advanced Batteries of Ministry of Education, College of Physics, Jilin University, Changchun 130012, China

(Dated: October 24, 2023)

Metal borides have been considered as potential high-temperature superconductors since the discovery of record-holding 39 K superconductivity in bulk MgB_2 . In this work, we identified a superconducting yet thermodynamically stable $F\bar{4}3m$ Sr_2B_5 at 40 GPa with a unique covalent sp^3 -hybridized boron framework through extensive first-principles structure searches. Remarkably, solving the anisotropic Migdal-Eliashberg equations resulted in a high superconducting critical temperature (T_c) around 100 K, exceeding the boiling point (77 K) of liquid nitrogen. Our in-depth analysis revealed that the high-temperature superconductivity mainly originates from the strong coupling between the metalized σ -bonded electronic bands and E phonon modes of boron atoms. Moreover, anharmonic phonon simulations suggest that $F\bar{4}3m$ Sr_2B_5 might be recovered to ambient pressure. Our current findings provide a prototype structure with a full σ -bonded boron framework for the design of high- T_c superconducting borides that may expand to a broader variety of lightweight compounds.

PACS numbers:

The quest for high-temperature superconductors has been the long-sought target since the discovery of superconductivity in solid mercury in 1911 [1]. According to the Bardeen-Cooper-Schrieffer (BCS) theory of superconductivity, light-element compounds are considered as promising candidates for high superconducting critical temperature (T_c) superconductors since they possess high Debye temperature, which is proportional to the T_c [2]. Recently, the theory-orientated experiments have established near-room-temperature superconductivity in a class of hydrides at high pressure, such as H_3S , LaH_{10} , and CaH_6 [3–10]. Nevertheless, the pressure required to realize these superconducting hydrides is exceptionally high and challenging to achieve. Therefore, it is of significant importance to search for alternative high- T_c superconductors at moderate pressures and even at ambient pressure for practical applications.

At low pressure, MgB_2 is the BCS superconductor with the highest T_c of 39 K owing to its high Debye temperature and strong electron-phonon coupling (EPC), primarily originating from the metalized σ -bonding bands of in-plane sp^2 -hybridized boron atoms [11, 12]. Thus, metal borides characterized by metallic σ bonds have attracted considerable attention in searching for high- T_c superconductors. Besides MgB_2 , a class of MB_2 , MB_6 , and MB_{12} (M represents transition metals) have also been experimentally identified to be superconducting with T_c below 20 K at ambient pressure [13–16]. Recently, Pei *et al.* discovered that α - MoB_2 , isostructural with MgB_2 , exhibits the second-highest T_c of 32 K at 100 GPa among all known borides [17]. However, as the main contribution at the Fermi level of these borides is not derived from σ bonds of boron atoms, none of them have achieved a T_c surpassing that of MgB_2 yet.

In addition to experiments, much effort has also been devoted to theoretical investigations to design borides with high T_c . On one hand, thermodynamically stable boride superconductors, such as BeB_6 , CaB , and SrB characterized by deformed sp^2 -hybridization [18–20], exhibit lower T_c compared to MgB_2 due to the weaker metallic σ bonds, which is similar to the experimental observation. On the other hand, a series of MB_2 monolayer and MB_4 trilayers, such as AlB_2 , MgB_4 , and InB_4 [21–23], have been predicted to exhibit high T_c due to the strong metallic σ bonds originating from sp^2 -hybridized boron atoms, while their producibility is unclear since their thermodynamic stability remains unknown. Similarly, various metastable sp^3 -hybridized borocarbides and boronitrides have also been predicted to exhibit higher T_c than MgB_2 [24–29], although none of them has been experimentally synthesized to date. Thus, it is encouraging to design metal borides with favorable thermodynamic stability and strong metallic sp^2/sp^3 σ -bonding characteristics that may lead to synthesizable high-temperature superconductors with a T_c higher than MgB_2 .

In this work, we performed a comprehensive first-principles structure searches for the alkaline-earth (AE) metal borides (M_xB_y , M = Mg, Ca, Sr, Ba, $x = 1-3$, $y = 1-8$) at pressures below 100 GPa via the swarm intelligence-based CALYPSO method [30, 31]. Besides the reproduced already known phases [19, 20, 32, 33], we predicted several new thermodynamically stable borides under high pressures. Among them, the $F\bar{4}3m$ Sr_2B_5 consists of a unique fully sp^3 -hybridized σ -bonded boron framework, where the density of states at Fermi level is mainly contributed by σ -bond. This results in a high T_c above 100 K, not only surpassing the boiling temperature (77 K) of liquid nitrogen but also setting a new record for the highest T_c among all known thermodynamically stable boride

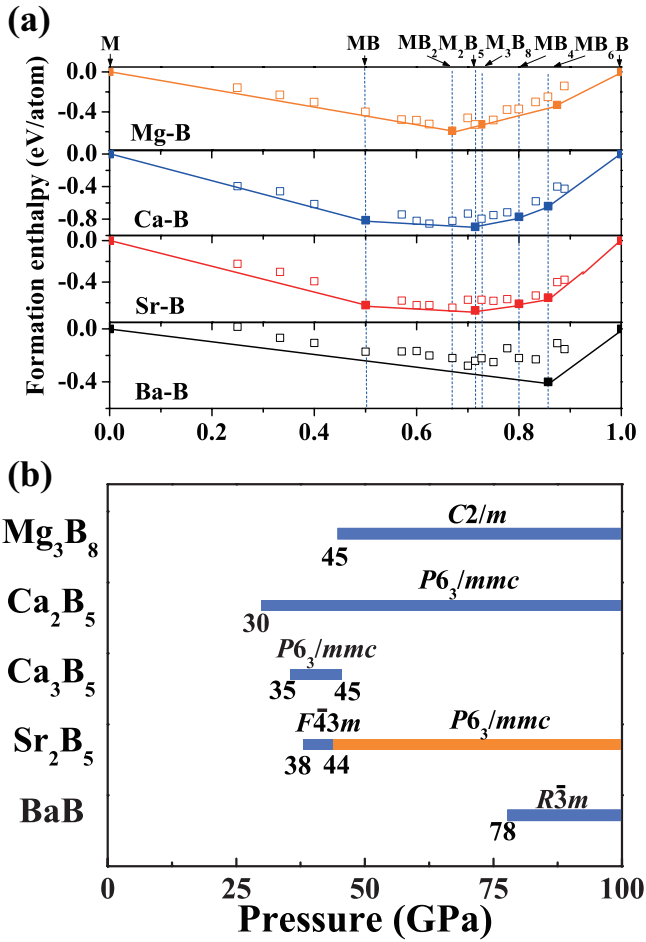


FIG. 1: (Color online) Phase stabilities of various AE borides M_xB_y ($M = \text{Mg, Ca, Sr, Ba}$, $x = 1-3$, $y = 1-8$) (a) Convex hull diagrams for M_xB_y at 50 GPa. (b) Pressure-composition phase diagram of newly-predicted Mg_3B_8 , Ca_2B_5 , Ca_3B_5 , Sr_2B_5 , and BaB .

superconductors.

Our main structure searching results of AE-metal borides M_xB_y below 100 GPa are presented in the convex hull and phase diagrams of Fig. 1 and Fig. S1 [34]. Considering the important contribution of zero-point energy (ZPE) to the free energy of compounds containing light elements [35, 36], the formation energies of the metal borides were calculated with the inclusion of ZPE. In addition to the known AE-metal borides [19, 20, 32, 33], we uncovered several new thermodynamically stable M_xB_y compounds, including Mg_3B_8 , Ca_2B_5 , Ca_3B_5 , Sr_2B_5 , and BaB with $C2/m$, $P6_3/mmc$, $P6_3/mmc$, $F\bar{4}3m$, and $R\bar{3}m$ structure, respectively, where Sr_2B_5 further transforms into $P6_3/mmc$ phase at 44 GPa (The detailed structural information is listed in Table S1 [34]). The absence of imaginary frequency in the phonon spectra indicates that these borides are also dynamically stable (Fig. S2 [34]), confirming the robustness of the stability. By examining the structures, we found that, except for $F\bar{4}3m\text{-Sr}_2\text{B}_5$, all the M_xB_y compounds adopt layered-like morphology with alternatively

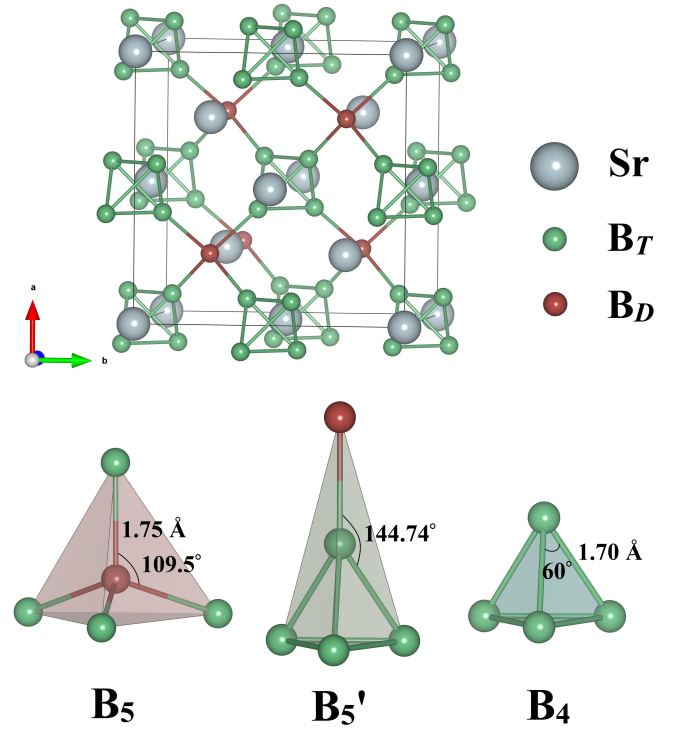


FIG. 2: (Color online) The side view of the structure of $F\bar{4}3m\text{-Sr}_2\text{B}_5$ at 40 GPa. The large and small spheres represent the Sr and B atoms, respectively.

stacked boron and metal atomic layers (Fig. S3 [34]). The boron atoms should be mainly sp^2 -hybridized in these M_xB_y compounds like other layered metal borides [18–20]. On the other hand, $F\bar{4}3m\text{-Sr}_2\text{B}_5$ exhibits a unique three-dimensional boron framework as presented in Fig. 2. It consists of two nonequivalent boron atoms, namely B_D and B_T , occupying $4c$ (0.25, 0.25, 0.25) and $16e$ (0.59, 0.59, 0.41) Wyckoff position, respectively, where both of them are four coordinated. Specifically, B_D is surrounded by four B_T atoms, which forms a regular tetrahedron B_5 unit similar to C atoms in diamond, indicating B_D is sp^3 -hybridized. B_T has three shorter $B_T\text{-}B_T$ bonds and one slightly longer $B_T\text{-}B_D$ bond and forms an irregular tetrahedron B_5' unit, in which B_T atoms also form a regular tetrahedron B_4 unit by itself. This is close to the motif of C atoms in T-carbon [37, 38], implying B_T exhibits resembling anisotropic sp^3 -hybridization due to the unevenly distributed bond lengths. Further electron localization function (ELF) and crystal orbital Hamiltonian population (COHP) calculations confirm the strong covalent nature between B atoms (Fig. S4 [34]). Meanwhile, Sr-B is ionically bonded since electrons are transferred from Sr to B. Remarkably, the boron sublattice of $F\bar{4}3m\text{-Sr}_2\text{B}_5$ can be viewed as isostructure to diamond, where one of the nonequivalent atomic position is occupied by B_4 unit instead of B atom. Thus, to the best of our knowledge, $F\bar{4}3m\text{-Sr}_2\text{B}_5$ should be the first metal boride exhibits fully sp^3 -hybridized σ -bonded boron framework that might be beneficial to the superconductivity.

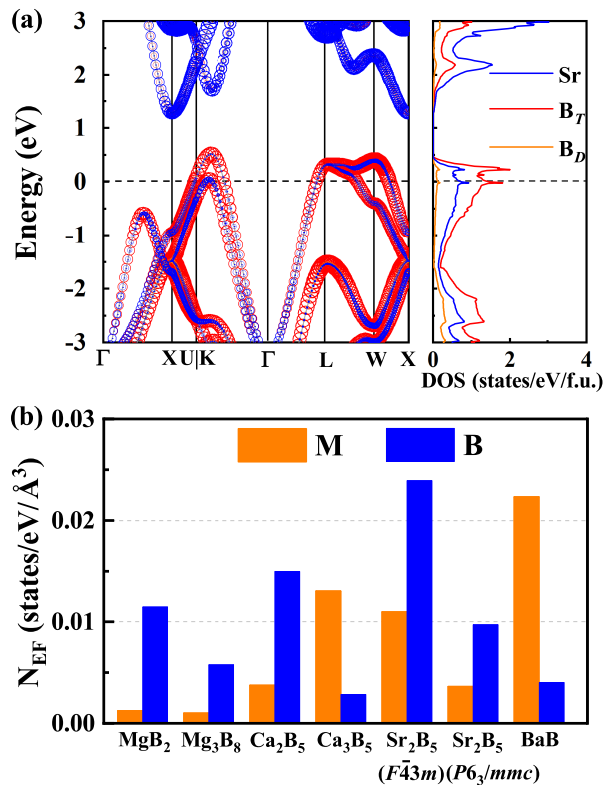


FIG. 3: (Color online) (a) Band structure and DOS of $F\bar{4}3m$ Sr₂B₅ at 40 GPa. (b) The projected density of states (PDOS) of boron atoms at the Fermi level in MgB₂, Mg₃B₈, Ca₂B₅, Ca₃B₅, $F\bar{4}3m$ Sr₂B₅, $P6_3/m\bar{m}c$ Sr₂B₅, and BaB at 0, 50, 30, 40, 40, 50, and 80 GPa, respectively.

We next examined the electronic properties of the AE-metal borides by modeling the band structures and density of states (DOS) as shown in Fig. 3 and Fig. S5 [34]. Clearly, the newly predicted metal borides are all metallic. Based on the boron hybridization scheme, these borides exhibit different band structure characteristics. The layered-like M_xB_y compounds have both σ and π bands crossing the Fermi level and $F\bar{4}3m$ -Sr₂B₅ only has σ conducting bands, analogous to that of MgB₂ and hole-doped diamond, respectively. Besides the metal-rich Ca₃B₅ and BaB, boron dominates the contribution to the DOS at the Fermi level (N_{Ef}) due to the charge transfer from metal to boron atoms, as deciphered in Fig. 3b. In the case of metal-rich borides, the amount of electrons provided by the metal atoms exceeds the needs of fully shelled boron atoms. Thus, N_{Ef} is dominated by metal atoms. Importantly, among these metal borides, $F\bar{4}3m$ Sr₂B₅ exhibits not only the highest total N_{Ef} but also the highest boron contribution, which is almost twice as much as that of MgB₂. This is because the Fermi level is located right at the peak position of the DOS, corresponding to a van Hove singularity along the K- Γ direction. The projected DOS further reveals that the electrons in the vicinity of the Fermi level are coming

from B_T, where B_D merely contributes to the N_{Ef} because it is nearly fully shelled due to the ideal sp^3 -hybridization. The high N_{Ef} together with the solely σ characteristic of boron suggest $F\bar{4}3m$ Sr₂B₅ should be a potential high-temperature superconductor if σ electronic bands couple strongly to the corresponding phonon modes. We also noticed that Ca₂B₅ has a boron contributed N_{Ef} higher than that of MgB₂. However, it is a mixture of σ and π electrons. The superconductivity of Ca₂B₅ might not be able to surpass that of MgB₂.

To investigate the potential superconductivity in these AE-metal borides, electron-phonon coupling simulations were performed. Encouragingly, the estimated EPC parameters, λ , of $F\bar{4}3m$ Sr₂B₅ is as high as 3.32 at 40 GPa. This value not only is nearly 3-4 times higher than that of MgB₂ but also higher than that of any sp^3 -hybridized borocarbides studied so far and close to that of high- T_c clathrate superhydrides. As depicted in Fig. 4(a), the large coupling strength is derived primarily from the T_2 and E modes over the whole Brillouin zone, which corresponded to the stretching of Sr-B bonds (2-7 THz) and rocking vibrations of B₄ units (8-10 THz). The integral ($\lambda(\omega)$) of the frequency divided Eliashberg phonon spectral function ($\alpha^2F(\omega)/\omega$) suggests these two modes contribute almost equally to the overall λ . This phenomenon is different from MgB₂ and metal borocarbides but similar to α -MoB₂ as metal atom shows pronounced contribution to N_{Ef} . Since the electron-phonon coupling is quite strong in $F\bar{4}3m$ Sr₂B₅ ($\lambda > 1.5$), the T_c values and superconducting energy gaps (Δ) were evaluated through the direct numerical solutions of the anisotropic Migdal-Eliashberg equations [39–41] using the calculated logarithmic average frequency (ω_{log}) and typical Coulomb potential parameters (μ^*) of 0.1, 0.13, and 0.16. The estimated single σ gap is about 22 meV (Fig. S8 [34]) and T_c value is 105 K using $\mu^* = 0.13$ for $F\bar{4}3m$ Sr₂B₅ at 40 GPa (Fig. 4), tripling that of MgB₂ and validating the observation of λ (those for $\mu^* = 0.1, 0.16$ are also provided in Fig.4 and Table S3 [34]). This predicted T_c certainly exceeds the boiling point of liquid-nitrogen (77 K), setting a new superconducting record among all known thermodynamically stable metal borides to the best of our knowledge.

Given the low mass of B, previous studies have demonstrated that anharmonicity played an important role in determining the superconductivity of MgB₂, especially for the E_{2g} phonons [42–44]. We then carried out additional EPC calculations to investigate the occurrence of anharmonic effects using the stochastic self-consistent harmonic approximation [45]. As shown in Fig. 4, the anharmonic correction only hardens and broadens the B₄ rocking E modes, while other phonon modes barely change, similar to that of MgB₂. The average phonon frequency of E modes increases from 9.3 THz to 11.6 THz and the width of E modes is increased by 1 THz. Meanwhile, E modes become the major contributor to the anharmonic Eliashberg function, accounting for 71% of total λ^{anh} , while the contribution of T_2 modes reduces to 25%, indicating the superconductivity of $F\bar{4}3m$ Sr₂B₅ should be mainly determined by the coupling between σ bands and E phonons. This results in a reduction of the anharmonic EPC parameter

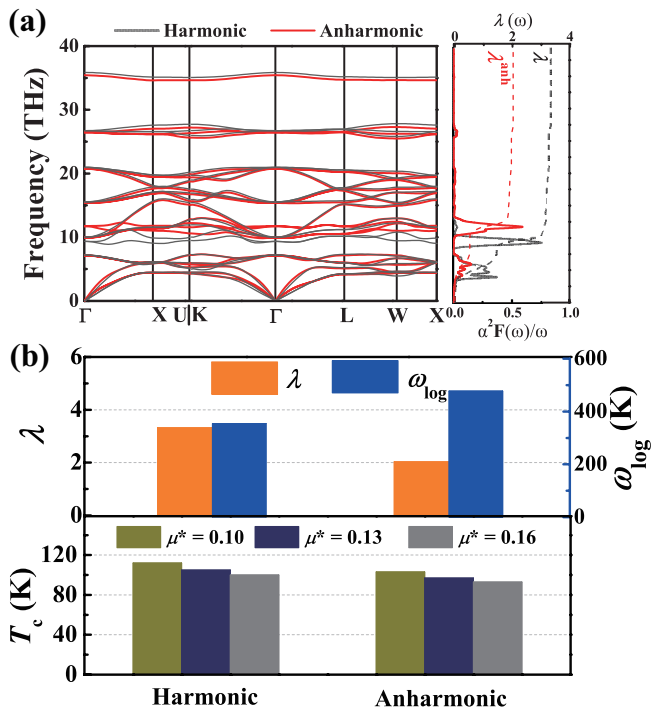


FIG. 4: (Color online) (a) Phonon dispersion relations, Eliashberg spectral function, (b) the electron-phonon coupling parameter λ , the logarithmic average frequency ω_{\log} and the superconducting temperature T_c of $F\bar{4}3m$ Sr_2B_5 by performing harmonic and anharmonic calculations at 40 GPa.

λ^{anh} to 2.02, 40% smaller than the harmonic one. In contrast, the anharmonicity enhances the logarithmic average frequency ω_{\log} by 34% from 354 K to 477 K. Consequently, the anharmonic T_c^{anh} value is dropped by 10% to 95 K, which still is quite high.

As for other newly predicted borides, only Ca_2B_5 , $P6_3/mmc$ Sr_2B_5 , and BaB exhibit superconductivity, with calculated T_c values of 3.6 K, 6.4 K, and 3.9 K at 30, 50, and 80 GPa, respectively. The details of superconducting properties are shown in Table S4 [34].

The high-temperature superconductivity of $F\bar{4}3m$ Sr_2B_5 drives us to further evaluate its synthesizability. As shown in Fig. S10 [34], the pressure-temperature phase diagram of Sr_2B_5 was constructed up to 100 GPa and 2000 K via harmonic free-energy calculations since most of the metal borides are synthesized at high temperatures [46]. Clearly, once temperature effects are considered, the stable range of $F\bar{4}3m$ Sr_2B_5 increases from 38-44 GPa at 0 K to 34-65 GPa at 2000 K, suggesting high temperature is good for the stabilization of $F\bar{4}3m$ Sr_2B_5 . Thus, $F\bar{4}3m$ Sr_2B_5 could be synthesized at moderate pressure by the large-volume press (LVP) since its stable range lies within the operating pressure and temperature range of LVP [47]. Compared to high- T_c BCS hydride superconductors, which can only be realized by the diamond anvil cell with micrometer-sized samples, the production of $F\bar{4}3m$ Sr_2B_5 shows a certain advantage as LVP can provide much

larger millimeter-sized samples for structure characterization and properties measurements. Moreover, we also found $F\bar{4}3m$ Sr_2B_5 is dynamically stable down to ambient pressure with anharmonic corrections (Fig. S11 [34]), implying it might be able to retain to 0 GPa with the proper quenching method. The T_c^{anh} of $F\bar{4}3m$ Sr_2B_5 at 0 GPa is predicted to be even higher around 115 K (Fig. S12 [34]).

As part of efforts to develop high-temperature BCS superconductors, we designed a promising thermodynamically stable $F\bar{4}3m$ Sr_2B_5 with record-high T_c at moderate synthetic pressure (~ 40 GPa). We note this is the first fully metallic sp^3 -hybridized boron framework example of metal borides, and we emphasize that the established B-B σ bonding is a key to achieving high- T_c at low pressures. For instance, if B_D atom is also replaced by the strongly coupled B_4 unit in $F\bar{4}3m$ Sr_2B_5 , the T_c might be even higher. Further investigation of other metal borides and lightweight compounds consisting of similar σ -bonding frameworks is expected which may lead to the discovery of potential high- T_c BCS superconductor (> 77 K) at ambient pressure.

In conclusion, our extensive first-principles structure searches for AE-metal (Mg, Ca, Sr, Ba) borides have revealed the appearance of stable Mg_3B_8 , Ca_2B_5 , Ca_3B_5 , Sr_2B_5 , and BaB below 100 GPa. Among them, $F\bar{4}3m$ Sr_2B_5 consisting of fully metallic sp^3 -hybridized B-B σ bonds exhibits potential high- T_c of 105 K at 40 GPa, with the possibility retaining to ambient pressure, that originates from the strong coupling between σ electronic bands and rocking vibrations of B_4 units. This unique boron framework resembles the diamond structure, serving as a design guidance for future investigation. Our results provide a useful structural prototype for designing high-temperature superconductors at low pressures and will stimulate further experimental synthesis and theoretical predictions for a large variety of metallic sp^3 -hybridized lightweight compounds.

This work is supported by by National Key Research and Development Program of China (Grant No. 2022YFA1402304), the National Natural Science Foundation of China (Grant no. 12022408, 12374008, 1202290458, 52288102, 52090024, 12074138, 12374007), the Interdisciplinary Integration and Innovation Project of JLU, Fundamental Research Funds for the Central Universities, Program for Jilin University Science and Technology Innovative Research Team (2021TD-05), Jilin Province Science and Technology Development Program (Grant No. YDZJ202102CXJD016), the Strategic Priority Research Program of Chinese Academy of Sciences (Grant No. XDB33000000) and computing facilities at the High-Performance Computing Centre of Jilin University.

* Electronic address: xieyu@jlu.edu.cn

† Electronic address: hanyuliu@jlu.edu.cn

‡ Electronic address: mym@jlu.edu.cn

- [1] H. K. Onnes, *Commun. Phys. Lab. Univ. Leiden*, b **120** (1911).
- [2] H. Suhl, B. Matthias, and L. Walker, *Phys. Rev. Lett.* **3**, 552 (1959).
- [3] A. Drozdov, M. Eremets, I. Troyan, V. Ksenofontov, and S. I. Shylin, *Nature* **525**, 73 (2015).
- [4] F. Peng, Y. Sun, C. J. Pickard, R. J. Needs, Q. Wu, and Y. Ma, *Phys. Rev. Lett.* **119**, 107001 (2017).
- [5] A. Drozdov, P. Kong, V. Minkov, S. Besedin, M. Kuzovnikov, S. Mozaffari, L. Balicas, F. Balakirev, D. Graf, V. Prakapenka, et al., *Nature* **569**, 528 (2019).
- [6] M. Somayazulu, M. Ahart, A. K. Mishra, Z. M. Geballe, M. Baldini, Y. Meng, V. V. Struzhkin, and R. J. Hemley, *Phys. Rev. Lett.* **122**, 027001 (2019).
- [7] L. Ma, K. Wang, Y. Xie, X. Yang, Y. Wang, M. Zhou, H. Liu, X. Yu, Y. Zhao, H. Wang, et al., *Phys. Rev. Lett.* **128**, 167001 (2022).
- [8] Y. Li, J. Hao, H. Liu, Y. Li, and Y. Ma, *J. Chem. Phys.* **140**, 174712 (2014).
- [9] H. Liu, I. I. Naumov, R. Hoffmann, N. Ashcroft, and R. J. Hemley, *Proc. Natl. Acad. Sci. U.S.A.* **114**, 6990 (2017).
- [10] H. Wang, J. S. Tse, K. Tanaka, T. Iitaka, and Y. Ma, *Proc. Natl. Acad. Sci. U.S.A.* **109**, 6463 (2012).
- [11] J. Nagamatsu, N. Nakagawa, T. Muranaka, Y. Zenitani, and J. Akimitsu, *Nature* **410**, 63 (2001).
- [12] J. Kortus, I. Mazin, K. D. Belashchenko, V. P. Antropov, and L. Boyer, *Phys. Rev. Lett.* **86**, 4656 (2001).
- [13] Z. Fisk, A. Lawsom, B. Matthias, and E. Corenzwit, *Phys. Lett. A* **37**, 251 (1971).
- [14] R. Schneider, J. Geerk, and H. Rietschel, *Europhys. Lett.* **4**, 845 (1987).
- [15] R. Lortz, Y. Wang, U. Tutsch, S. Abe, C. Meingast, P. Popovich, W. Knafo, N. Shitsevalova, Y. B. Paderno, and A. Junod, *Phys. Rev. B* **73**, 024512 (2006).
- [16] G. Akopov, M. T. Yeung, and R. B. Kaner, *Adv. Mater.* **29**, 1604506 (2017).
- [17] C. Pei, J. Zhang, Q. Wang, Y. Zhao, L. Gao, C. Gong, S. Tian, R. Luo, M. Li, W. Yang, et al., *Natl. Sci. Rev.* **10**, nwad034 (2023).
- [18] L. Wu, B. Wan, H. Liu, H. Gou, Y. Yao, Z. Li, J. Zhang, F. Gao, and H.-K. Mao, *J. Phys. Chem. Lett.* **7**, 4898 (2016).
- [19] Z. Cui, Q. Yang, X. Qu, X. Zhang, Y. Liu, and G. Yang, *J. Mater. Chem. C* **10**, 672 (2022).
- [20] S. Shah and A. N. Kolmogorov, *Phys. Rev. B* **88**, 014107 (2013).
- [21] Y. Zhao, C. Lian, S. Zeng, Z. Dai, S. Meng, and J. Ni, *Phys. Rev. B* **100**, 094516 (2019).
- [22] Y. Zhao, C. Lian, S. Zeng, Z. Dai, S. Meng, and J. Ni, *Phys. Rev. B* **101**, 104507 (2020).
- [23] Z. Wang, S. Zeng, Y. Zhao, X. Wang, and J. Ni, *Phys. Rev. B* **104**, 174519 (2021).
- [24] N. Geng, K. P. Hilleke, L. Zhu, X. Wang, T. A. Strobel, and E. Zurek, *J. Am. Chem. Soc.* (2023).
- [25] T. T. Gai, P. J. Guo, H. C. Yang, Y. Gao, M. Gao, and Z. Y. Lu, *Phys. Rev. B* **105**, 224514 (2022).
- [26] H. B. Ding, Y. J. Feng, M. J. Jiang, H. L. Tian, G. H. Zhong, C. L. Yang, X. J. Chen, and H. Q. Lin, *Phys. Rev. B* **106**, 104508 (2022).
- [27] L. Zhu, G. M. Borstad, H. Liu, P. A. Guńka, M. Guerette, J.-A. Dolyniuk, Y. Meng, E. Greenberg, V. B. Prakapenka, B. L. Chou, et al., *Sci. Adv.* **6**, eaay8361 (2020).
- [28] P. Zhang, X. Li, X. Yang, H. Wang, Y. Yao, and H. Liu, *Phys. Rev. B* **105**, 094503 (2022).
- [29] J.-N. Wang, X.-W. Yan, and M. Gao, *Phys. Rev. B* **103**, 144515 (2021).
- [30] Y. Wang, J. Lv, L. Zhu, and Y. Ma, *Phys. Rev. B* **82**, 094116 (2010).
- [31] Y. Wang, J. Lv, L. Zhu, and Y. Ma, *Comput. Phys. Commun.* **183**, 2063 (2012).
- [32] M. M. D. Esfahani, Q. Zhu, H. Dong, A. R. Oganov, S. Wang, M. S. Rikitin, and X. F. Zhou, *Phys. Chem. Chem. Phys.* **19**, 14486 (2017).
- [33] A. Kolmogorov, S. Shah, E. Margine, A. Kleppe, and A. Jephcoat, *Phys. Rev. Lett.* **109**, 075501 (2012).
- [34] See Supplemental Material at <https://XXX> for computational details, formation enthalpies, phase diagrams, electronic structures, phonon dispersion curves, superconducting properties, and structural information of alkline-earth borides, which includes Refs. [30, 31, 40, 46, 48-62]
- [35] C. H. Hu, A. R. Oganov, Q. Zhu, G. R. Qian, G. Frapper, A. O. Lyakhov, and H. Y. Zhou, *Phys. Rev. Lett.* **110**, 165504 (2013).
- [36] F. Peng, M. Miao, H. Wang, Q. Li, and Y. Ma, *J. Am. Chem. Soc.* **134**, 18599 (2012).
- [37] X. L. Sheng, Q. B. Yan, F. Ye, Q. R. Zheng, and G. Su, *Phys. Rev. Lett.* **106**, 155703 (2011).
- [38] J. Zhang, R. Wang, X. Zhu, A. Pan, C. Han, X. Li, D. Zhao, C. Ma, W. Wang, H. Su, et al., *Nat. Commun.* **8**, 683 (2017).
- [39] G. M. Eliashberg, *Sov. Phys. JETP* **11**, 696 (1960).
- [40] A. Sanna, J. A. Flores-Livas, A. Davydov, G. Profeta, K. Dewhurst, S. Sharma, and E. Gross, *J. Phys. Soc. Japan* **87**, 041012 (2018).
- [41] F. Giustino, M. L. Cohen, and S. G. Louie, *Phys. Rev. B* **76**, 165108 (2007).
- [42] A. Y. Liu, I. Mazin, and J. Kortus, *Phys. Rev. Lett.* **87**, 087005 (2001).
- [43] T. Yildirim, O. Gülseren, J. Lynn, C. Brown, T. Udovic, Q. Huang, N. Rogado, K. Regan, M. Hayward, J. Slusky, et al., *Phys. Rev. Lett.* **87**, 037001 (2001).
- [44] M. Lazzeri, M. Calandra, and F. Mauri, *Phys. Rev. B* **68**, 220509 (2003).
- [45] I. Errea, M. Calandra, and F. Mauri, *Phys. Rev. B* **89**, 064302 (2014).
- [46] A. Friedrich, B. Winkler, E. A. Juárez-Arellano, and L. Bayarjargal, *Materials* **4**, 1648 (2011).
- [47] T. Ishii, Z. Liu, and T. Katsura, *Engineering* **5**, 434 (2019).
- [48] Y. Wang and J. P. Perdew, *Phys. Rev. B* **43**, 8911 (1991).
- [49] G. Kresse and J. Furthmüller, *Phys. Rev. B* **54**, 11169 (1996).
- [50] J. P. Perdew and Y. Wang, *Phys. Rev. B* **45**, 13244 (1992).
- [51] P. E. Blöchl, *Phys. Rev. B* **50**, 17953 (1994).
- [52] H. J. Monkhorst and J. D. Pack, *Phys. Rev. B* **13**, 5188 (1976).
- [53] A. Togo, F. Oba, and I. Tanaka, *Phys. Rev. B* **78**, 134106 (2008).
- [54] R. Dronskowski and P. E. Bloechl, *J. Phys. Chem.* **97**, 8617 (1993).
- [55] V. L. Deringer, A. L. Tchougréeff, and R. Dronskowski, *J. Phys. Chem. A* **115**, 5461 (2011).
- [56] S. Maintz, V. L. Deringer, A. L. Tchougréeff, and R. Dronskowski, *J. Comput. Chem.* **37**, 1030 (2016).
- [57] P. Giannozzi, S. Baroni, N. Bonini, et al., *J. Phys. Condens. Mat.* **21**, 395502 (2009).
- [58] G. Pizzi, V. Vitale, R. Arita, et al., *J. Phys. Condens. Mat.* **32**, 165902 (2020).
- [59] S. Poncé, E. R. Margine, C. Verdi, and F. Giustino, *Comput. Phys. Commun.* **209**, 116 (2016)
- [60] H. J. Choi, M. L. Cohen, and S. G. Louie, *Phys. C (Amsterdam, Neth.)* **385**, 66 (2003).
- [61] E. R. Margine and F. Giustino, *Phys. Rev. B* **87**, 024505 (2013).
- [62] S. D. Cataldo, W. V. D. Linden, L. Boeri, *Phys. Rev. B*, **102**, 014516 (2020).